CrystEngComm

RSC Publishing

PAPER

View Article Online
View Journal | View Issue

Cite this: *CrystEngComm*, 2013, **15**, 10043

Solar light photocatalysis using Bi_2O_3/Bi_2SiO_5 nanoheterostructures formed in mesoporous SiO_2 microspheres†

Ling Zhang, Wenzhong Wang,* Songmei Sun, Dong Jiang and Erping Gao

Received 19th July 2013,
Accepted 16th September 2013

DOI: 10.1039/c3ce41433g

www.rsc.org/crystengcomm

There have been significant efforts to find novel photocatalytic materials with improved properties, such as an extended absorption wavelength from the UV to the visible-light region. Among the semiconductors with high photocatalytic activities, considerable attention has been given to bismuth-based oxides with suitable band gaps, which provide an opportunity to harvest visible light. Herein, we report Bi_2O_3/Bi_2SiO_5 nanoheterostructures formed in mesoporous SiO_2 microspheres. The as-prepared nanocomposite exhibited excellent photocatalytic activities for the decomposition of both bisphenol A and acetaldehyde under irradiation by simulated solar light. The enhanced photocatalytic activity is due to (i) the reduction in the electron–hole recombination rate because of the reduced dimensions of the photocatalyst, (ii) a more efficient utilization of the photogenerated electrons and holes as a result of the high surface area to bulk ratio of the mesoporous structure, and (iii) a better electron–hole pair separation due to the formation of the Bi_2O_3/Bi_2SiO_5 nanoheterostructure. The high efficiency in the degradation of organic pollutants under mild conditions makes the as-prepared mesoporous photocatalyst a promising candidate for photocatalytic environmental purification.

Introduction

In recent years, there have been significant efforts to search for novel photocatalytic materials with improved properties, which consider the importance of photocatalysis in environmental remediation and energy conversion.[1–3] In particular, the fabrication of mesoporous photocatalysts has become a research hotspot because of their high photocatalytic activities due to the increase in the number of surface reactive sites and improved mass transport, resulting from the large surface areas, ordered porous structures and large pore volumes.[4–7] Metals (Au, Ag, Mo *etc.*) or metal oxides (TiO_2, Bi_2O_3, CuO) supported on mesoporous silica (*e.g.* MCM-41, SBA-15) have been used as photocatalysts to degrade organic dyes and NO_x.[5,8–13] On the other hand, increasing attention has been devoted to directly fabricating mesoporous semiconductor catalysts (*e.g.* TiO_2, WO_3, CeO_2) so as to enhance their performance to meet the requirements for practical applications.[4,14–19] However, photocatalysts which are supported on a mesoporous frame or have an intrinsic mesoporous structure, face several obstacles: (i) the excess nanocatalyst supported on the mesoporous frame can block the pores thus reducing the number of active sites and the surface area;[3] and (ii) thermal stability is a big problem for mesoporous structures of semiconductors because they are destroyed at high temperatures.[2,20] For example, it is well known that the fabrication of mesoporous titania with an ordered crystalline framework is a great challenge. The mesoporous framework of TiO_2 easily collapses during thermal treatment.[21,22] These obstacles limit the practical applications of mesoporous photocatalysts.

Herein, we addresses these problems by implementing a novel approach to synthesize a mesoporous photocatalyst possessing a high photocatalytic activity and high thermal stability. The case study includes the design, synthesis and characterization of Bi_2O_3/Bi_2SiO_5 nanoheterostructures dispersed in a mesoporous SiO_2 matrix. The reasons to work with this material are as follows:

First, bismuth-based oxides appear to be good candidates for visible light driven photocatalysts because their band gaps vary over a broad range. Bi_2O_3 with a band gap of 2.8 eV can oxidize water and generate highly reactive species for initiating oxidation reactions.[23–26] In addition, Bi_2SiO_5 has been reported as a good photocatalyst for the degradation of a dye pollutant.[27–32] Bi_2SiO_5 and Bi_2O_3 have been proved to be highly active photocatalysts under irradiation by UV and visible light, respectively.

Second, an effective way to enhance the photocatalytic activity is by coupling semiconductors with matching band

State Key Laboratory of High Performance Ceramics and Superfine Microstructures, Shanghai Institute of Ceramics, Chinese Academy of Sciences, 1295 Dingxi Road, Shanghai 200050, P. R. China. E-mail: wzwang@mail.sic.ac.cn; Tel: +86 21 5241 5295

† Electronic supplementary information (ESI) available. See DOI: 10.1039/c3ce41433g

gaps because of promoted electron–hole separations.[1,23,32–34] To couple Bi_2O_3 and Bi_2SiO_5, a heterojunction interface between the two semiconductors with matching band potentials would need to be constructed. Thus, advantages such as an improved charge separation, an increased lifetime of the charge carrier, and an enhanced interfacial charge transfer efficiency can be achieved.

In the present study, a Bi_2O_3/Bi_2SiO_5 coupled semiconductor was successfully introduced on the surface of a mesoporous SiO_2 microsphere matrix. Its photocatalytic activity was proved by the decomposition of bisphenol A (BPA) and acetaldehyde under irradiation by simulated sunlight. On the basis of the results achieved, it is believed that mesoporous bismuth-based oxide photocatalysts are excellent candidates for the degradation of various organic pollutants.

Experimental section

Materials

All the chemicals were purchased from Shanghai Reagent Co., Ltd. (China). They were used as received without further purification.

Synthesis of mesoporous SiO_2 microspheres

Following a typical method for synthesising mesoporous SiO_2 microspheres,[35] 0.26 g of Pluronic F127 and 0.65 g of FC-4 ($C_3F_7O(CFCF_3CF_2O)_2CFCF_3CONH(CH_2)_3N^+(C_2H_5)_2CH_3I^-$) were dissolved in 30 mL of HCl solution (0.02 M), followed by the introduction of 0.30 g of 1,3,5-trimethylbenzene (TMB). After stirring for 2 h, 1.5 g of tetraethyl orthosilicate (TEOS) were added. Then the solution was stirred at 30 °C for 24 h, transferred to an autoclave, and kept at 100 °C for 24 h. The as-synthesized material was collected using a centrifuge, dried in air, and heat treated at 550 °C for 5 h for surfactant removal.

Synthesis of the photocatalyst samples

Bismuth nitrate ($Bi(NO_3)_3{\cdot}5H_2O$) was dissolved in acetic acid. The SiO_2 powder prepared as above was added to the mixture solution (molar ratio Bi : Si = 0.15 : 1) and then the solution was dried at room temperature. The mixture in powder form was heat treated at 500 °C for 3 h in air. $Bi_2O_3/Bi_2SiO_5@SiO_2$ (M-BBS) was obtained after cooling down to room temperature.

In order to prepare the Bi_2SiO_5/SiO_2 (M-BS) sample, the $Bi_2O_3/Bi_2SiO_5@SiO_2$ powder was added to a HNO_3 solution (1 M) and stirred for 1 h. The as-synthesized material was collected using a centrifuge, and dried at 60 °C in air.

In a typical synthesis of pure Bi_2SiO_5, 0.94 g of $Bi(NO_3)_3{\cdot}5H_2O$ and 0.27 g of $Na_2SiO_3{\cdot}9H_2O$ were added into 30 mL of deionized water. Under vigorous stirring, the pH value of the mixture was adjusted to 9 by the dropwise addition of 10% $NH_3{\cdot}H_2O$. After stirring for 20 min, the mixture was transferred into a Teflon-lined autoclave with a capacity of 50 mL. Then, the autoclave was sealed, heated at 180 °C for 48 h, and then allowed to cool to room temperature naturally. The solid product was collected, washed with distilled water and absolute ethanol several times, and then dried at 80 °C for 8 h. A white Bi_2SiO_5 powder sample was obtained (denoted as HR-Bi_2SiO_5 (HR-B)).

In order to prepare the Bi_2SiO_5/Bi_2O_3 (HR-BB) sample, the as-prepared HR-B powder (0.26 g) and 0.0485 g of $Bi(NO_3)_3{\cdot}5H_2O$ were added into 30 mL of aqueous NaOH (1 M) and stirred for 30 min. The mixture was transferred into a Teflon-lined autoclave with a capacity of 50 mL. Then, the autoclave was sealed, heated at 180 °C for 24 h, and then allowed to cool to room temperature naturally. The solid product was collected, washed with distilled water and absolute ethanol several times, and then dried at 80 °C for 8 h. A yellow-white powder sample was obtained.

Characterization methods

Powder XRD patterns were collected on a Rigaku D/MAX-2550V diffractometer at 30 kV and 15 mA (Co Kα radiation). TEM analysis was performed using a JEOL 2100F electron microscope operated at 200 kV. N_2 adsorption–desorption isotherms were obtained using a Micromeritics Tristar 3000 pore analyzer at 77 K. BET and BJH analyses were used to determine the surface area, pore size, and pore volume.

Photocatalysis

The UV-vis absorption spectra were measured on a UV-vis spectrophotometer (Hitachi U-3010). The photocatalytic activity of the Bi_2SiO_5/SiO_2 mesoporous microspheres for the decomposition of BPA (20 mg L^{-1}) and CH_2O (400 ppm) were evaluated under irradiation by simulated sunlight (a 500 W Xe lamp). The initial concentration of BPA was 20 mg L^{-1} with a catalyst loading of 0.5 g L^{-1}. After the elapse of a definite time, a small quantity of the solution was taken out, and the concentrations of the pollutants were determined using a UV-vis spectrophotometer. Before the absorption measurement, the sample solutions were centrifuged at 5000 rpm for 10 min in order to remove the catalyst particles from the solutions. The absorption was converted to the pollutant's concentration by referring to a standard curve showing a linear behavior between the concentration and the absorption at a specific wavelength.

For the degradation of acetaldehyde (CH_3CHO), 0.1 g of the photocatalyst was placed on the bottom of a gas-closed reactor with a quartz window at room temperature (capacity 600 mL). The reaction gas mixture (1 atm) consisted of 400 ppm CH_3CHO and N_2 balance gas. Prior to irradiation, the reaction system was equilibrated for about 5 h until no change in the concentration of CO_2 was observed. Gaseous samples (1 mL) were periodically extracted and analyzed by a gas chromatograph (GC) equipped with a flame ionization detector (N_2 carrier) and a catalytic conversion furnace.

Results and discussion

Synthesis of the $Bi_2O_3/Bi_2SiO_5@SiO_2$ mesoporous microspheres

The M-BBS mesoporous microspheres were synthesized *via* a structure replication synthesis method. The synthesis process

involved several steps, as illustrated in Scheme 1. First, SiO_2 mesoporous spheres with a pore size of ~9.5 nm were prepared according to ref. 35. Second, the SiO_2 powder was immersed in a solution containing bismuth nitrate and acetic acid. The precursor infiltrated the pores of the SiO_2 mesoporous spheres in this process. Subsequently, the mixture was dried and heat treated to produce crystalline Bi_2O_3/Bi_2SiO_5 in the frame of the SiO_2 mesoporous microspheres. Furthermore, Bi_2O_3 could be dissolved by treating it with an aqueous solution of HNO_3. It is worth noting that the ratio of bismuth nitrate to SiO_2 is the key to obtaining $Bi_2O_3/Bi_2SiO_5@SiO_2$. If too much bismuth nitrate was introduced, a mixture of Bi_2O_3 and $Bi_{10}SiO_{24}$ would be present in the product, and the pore channels would be over filled.

Structure characterization

The morphology and mesoporous characteristics of the M-BBS were observed using transmission electronic microscopy (TEM). As shown in Fig. 1a, the diameter of the M-BBS spheres was several hundred nanometers. As shown in the inset of Fig. 1a, the mesoporous channels can be clearly observed; the wall thickness of the pore channel is ~5 nm and the mesopore size is estimated to be ~8.0 nm, which is smaller than that of the pure mesoporous SiO_2 matrix.[35] In addition, the opened pore structure of the as-prepared SiO_2 microspheres was also observed, which is helpful for the adsorption of the pollutant. The energy-dispersive X-ray (EDX) spectrum shown in Fig. 1b proves that the Bi ions were introduced into the SiO_2 mesoporous framework. As a comparison, the as-prepared HR-BB sample was a mixture of thin nanoplates with thicknesses of 10–20 nm and nanoparticles with diameters of 30–80 nm (see Fig. S1, ESI†).

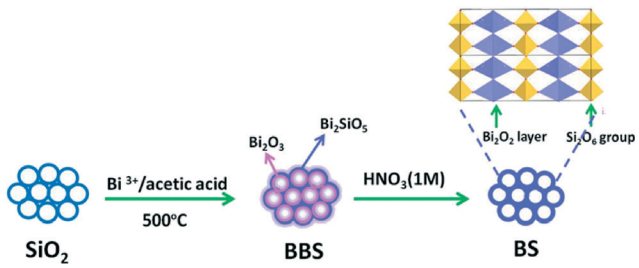

Scheme 1 Synthesis of mesostructured BBS and BS by Bi ions and a mesoporous SiO_2 microsphere framework.

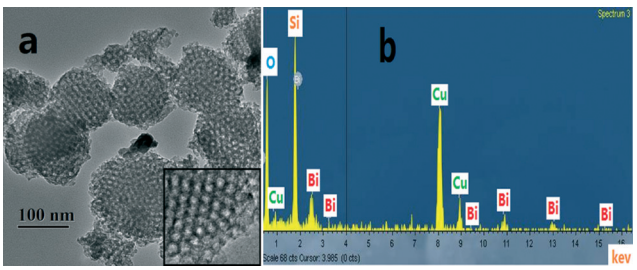

Fig. 1 (a) TEM image of the M-BBS sample, inset: enlarged pore structures; (b) EDX spectrum of the M-BBS sample taken from the area shown in (a).

The XRD patterns of the sample were recorded. As shown in Fig. 2, most of the observable peaks were indexed to the orthorhombic Bi_2SiO_5 phase (JCPDS: 36-0287) and the minor peaks were indexed to the Bi_2O_3 phase (JCPDS: 50-1088). This means that Bi_2SiO_5 was formed from the heat treatment of the Bi ions precursor within the mesoporous SiO_2 microspheres and Bi_2O_3 was formed on the surface of Bi_2SiO_5 from the reaction of excessive Bi with O_2 in the air. The mesoporous structure of BBS was confirmed by the low-angle XRD pattern (inset of Fig. 2). Combining the results from TEM and XRD implies that the M-BBS is thermally stable after heat treatment at 500 °C and the ordered mesoporous structure is partially preserved, though a few of the pores were over filled. The mean sizes of the Bi_2O_3 and Bi_2SiO_5 particles in the M-BBS sample calculated using the Scherrer equation and the XRD data were 21.4 nm and 14.6 nm, respectively.

Fig. 3 shows the N_2 adsorption–desorption isotherm and the corresponding Barrett–Joyner–Halenda (BJH) pore-size distribution plot (inset of Fig. 3) of the M-BBS. At relatively

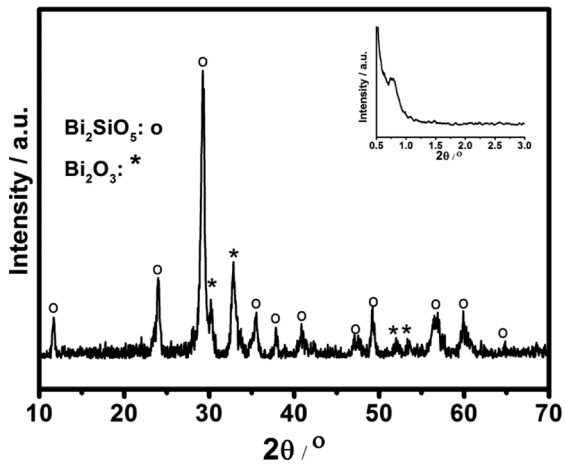

Fig. 2 XRD pattern of the M-BBS in the high-angle range (Bi_2SiO_5: ○, Bi_2O_3: *); inset: XRD pattern of the M-BBS in the low-angle range.

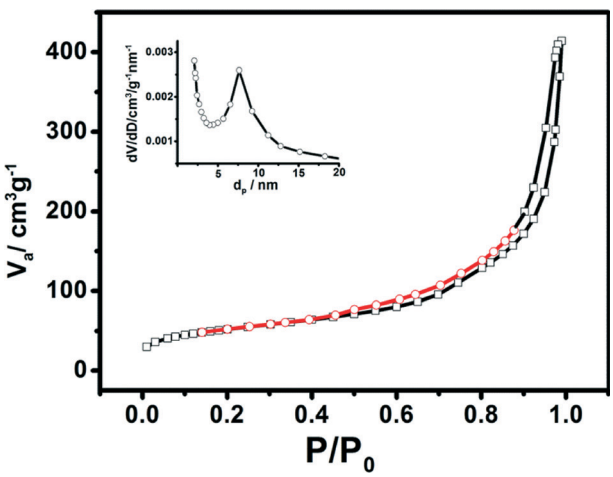

Fig. 3 N_2 adsorption–desorption isotherm of the M-BBS. Inset: the corresponding pore size distribution curve of the M-BBS sample calculated from the desorption branch of the isotherm by the BJH method.

high pressure, the curve exhibits a small hysteresis loop, which is attributed to a type IV isotherm and is representative of mesoporous materials. The M-BBS has a narrow BJH adsorption pore size distribution with a mean value of 7.5 nm, implying that the material has regular pore channels in the mesoporous region. Accordingly, the Brunauer–Emmett–Teller (BET) surface area was reduced from 306.8 $m^2\ g^{-1}$ to 187.08 $m^2\ g^{-1}$ for the SiO_2 and M-BBS samples, respectively. The difference in the surface area between the two samples can be explained by the pore sizes and density. First, the size of the crystal lattice of Bi_2SiO_5 was bigger than that of SiO_2. When the Bi ions entered the mesoporous framework, the wall thickness increased resulting in a reduction in the pore size. Second, the density of the bulk Bi_2SiO_5 (7.87 g cm^{-3}) is higher than that of bulk silica (2.26 g cm^{-3}), which must also be taken into account.

The light utilization efficiency, which greatly influences the photocatalytic performance, could be enhanced by introducing the visible light driven photocatalyst as a component of a heterostructure. The UV-vis diffuse reflection spectra (DRS) of the as-prepared samples are shown in Fig. 4. According to the spectrum, the photoresponse properties from the UV light region to ~385 nm result from Bi_2SiO_5, and the photoresponse properties from the visible light region to ~700 nm result from Bi_2O_3. The as-prepared photocatalyst shows a strong absorption in the ultraviolet region of 200–385 nm, and a slight absorption in the visible region. This reveals that Bi_2O_3/Bi_2SiO_5 can be used as a sunlight active semiconductor photocatalyst. Strong UV light absorption may lead to an increase in the generation of electron–hole pairs, which enhances the photocatalytic activity of the catalyst.[24] At the same time, the visible light absorption ability is advantageous for enhancing the usability of solar light. As a comparison, the DRS of the as-prepared HR-BB and HR-B are shown in the inset of Fig. 4.

Photocatalytic activity

Adsorption and enrichment of pollutants with low concentrations in solution are advantages of mesoporous structured materials. BPA is in low concentrations in surface water (including rivers and oceans), but it has an endocrine effect and is hardly degraded in the natural environment.[36,37] Here, the photocatalytic activity of the M-BBS was investigated by looking at the degradation of BPA as a target pollutant. BPA degradation efficiencies with different photocatalysts under otherwise identical conditions were measured. The results are shown in Fig. 5a, where C_t is the absorption of BPA at wavelength 274 nm and C_0 is the absorption of BPA after the adsorption equilibrium before irradiation. A blank test (BPA without any catalyst) under a Xe lamp exhibited no degradation, which indicates the photolysis of BPA could be ignored. When the M-BBS was used as the photocatalyst, 90% of BPA was degraded after 120 min under a Xe lamp, which shows it has a better photocatalytic activity than that of P25 (TiO_2). However, after 120 min, the degraded BPA by the M-BS and HR-BB were only about 30 and 38%, respectively. Obviously, the photocatalytic activity of the M-BBS is higher compared to the M-BS and HR-BB.

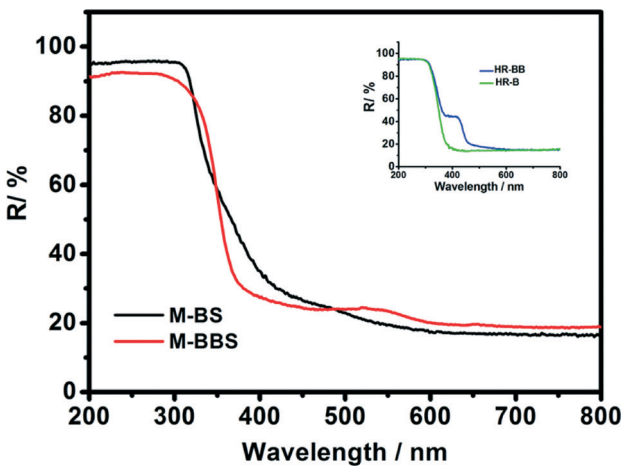

Fig. 4 UV-vis diffuse reflectance spectra for the as-prepared M-BS and M-BBS samples. Inset: DRS of the HR-B and HR-BB samples.

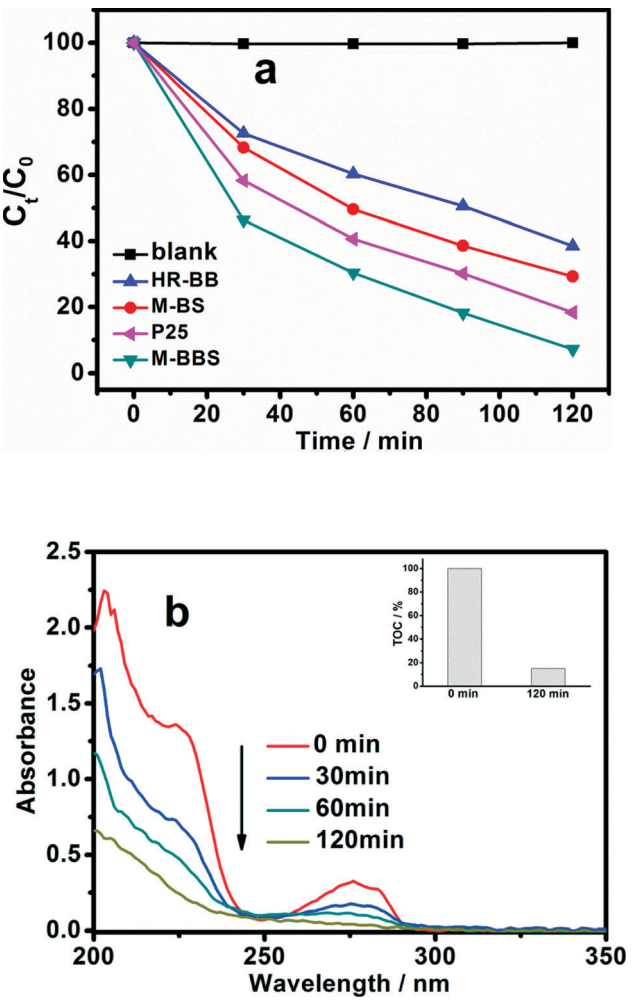

Fig. 5 (a) Photodegradation efficiencies of BPA as a function of irradiation time by different photocatalysts; (b) UV spectral changes of an aqueous solution of BPA containing a M-BBS suspension as a function of irradiation time. The inset shows the variation of the TOC value in the BPA aqueous solution over the irradiation time.

Fig. 5b displays the temporal evolution of the spectral changes during the photodegradation of BPA over the M-BBS sample. A rapid decrease in the BPA absorption at the wavelength of 274 nm within 30 min was observed. The mineralization of the pollutant was investigated by measuring the decrease in the total organic carbon (TOC) during the photodegradation process. As shown in the inset of Fig. 5b, the TOC value decreased by about 85% after irradiation for 120 min. This confirms that most of the BPA molecules were mineralized into CO_2 and H_2O, further demonstrating the high photocatalytic activity of the M-BBS.

The possibility of reusing the photocatalyst was explored. Experimental results demonstrated that the recycled photocatalyst achieved the successful removal of BPA as shown in Fig. S3, ESI.†

Besides the decomposition of organic pollutants in solution, the photocatalytic degradation of acetaldehyde, a typical indoor air contaminant, was also performed under irradiation by a Xe lamp. Since it is also a common intermediate during the photocatalytic oxidation of other organic compounds ranging from alkanes to alcohols, the mineralization of acetaldehyde is significant to the application of photocatalysts in deep purification.[38] It was revealed that acetaldehyde was degraded by the sample with an obvious production of CO_2 (Fig. 6). The rate of CO_2 evolution over the M-BBS composite photocatalyst was much higher than that over the M-BS sample. The blank test showed that no self-decomposition existed, which strongly confirmed the effect of photocatalytic degradation by the M-BBS photocatalyst.

Mechanism of photocatalytic degradation

A possible mechanism for the high photocatalytic activity of the $Bi_2O_3/Bi_2SiO_5@SiO_2$ photocatalyst is proposed in Scheme 2. Three main reasons for the increase in the photocatalytic efficiency of the Bi_2O_3/Bi_2SiO_5 nanoheterostructure are: (i) the reduction in the electron–hole recombination rate because of the reduced dimensions of the photocatalyst. The size of the

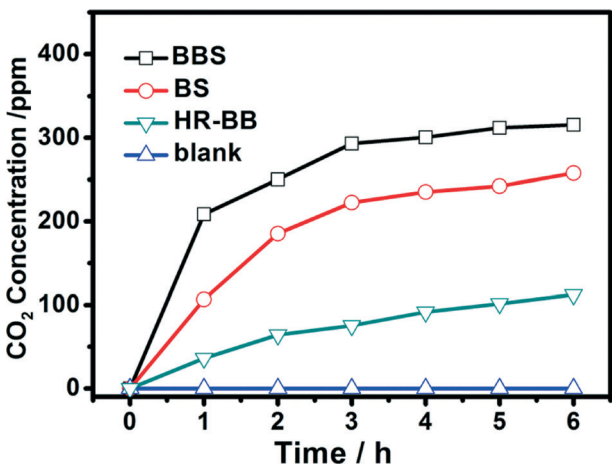

Fig. 6 Acetaldehyde degradation in the presence of different photocatalysts under irradiation by simulated sunlight.

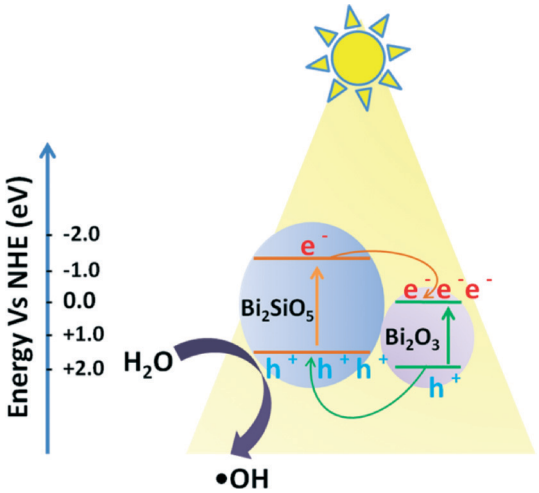

Scheme 2 Mechanism of photocatalytic degradation.

$Bi_2O_3/Bi_2SiO_5@SiO_2$ photocatalyst (~5 nm wall thickness of the pore channel) is comparable to the Debye length of bismuth oxide,[39–41] which means that the minority carriers generated within a few nanometers from the surfaces of the nanocomposite would escape recombination and take part in the surface reaction. (ii) The more efficient consumption of photogenerated electrons and holes as a result of the high surface area to bulk ratio of the mesoporous structure. This provides a shorter path for the diffusive transport of electrons and holes to the surfaces of the photocatalyst, also making the recombination of electrons and holes less probable. (iii) The efficient electron–hole pair separation due to the formation of Bi_2O_3/Bi_2SiO_5 nanoheterostructures. The relative energy levels of the Bi_2O_3/Bi_2SiO_5 coupled system are given in Scheme 2 (according to the DFT calculation results).[26,28] The excited electrons are transferred from Bi_2SiO_5 to Bi_2O_3whereas holes on Bi_2O_3 migrate to Bi_2SiO_5, which facilitates the charge separation and higher photocatalytic efficiency. This process not only facilitates the charge separation but also accumulates holes in Bi_2SiO_5. In the photocatalytic process induced by Bi_2SiO_5, it has been proved that the photogenerated holes react with adsorbed water to form $^{\bullet}OH$ radicals, which are the major active oxidation species in the decomposition of organic pollutants.[31] Furthermore, there was no $O_2^{\bullet-}$ detected in the irradiated M-BBS aqueous suspensions (see Fig. S2, ESI†).

Conclusions

A novel $Bi_2O_3/Bi_2SiO_5@SiO_2$ composite with a mesoporous structure was successfully synthesized through a SiO_2 template replication method, using bismuth nitrate as the precursor. The as-prepared M-BBS facilitates excellent photocatalytic decomposition reactions of BPA and acetaldehyde under irradiation by simulated sunlight. Comparative studies indicated that the photocatalytic performance of the M-BBS sample was much higher than that of the M-BS and HR-BB samples under the same conditions. The high photocatalytic activity is ascribed to (i) the reduction in the electron–hole recombination

rate because of the reduced dimensions of the photocatalyst; (ii) a more efficient consumption of the photogenerated electrons and holes as a result of the high surface area to bulk ratio of the mesoporous structure; and (iii) a better electron–hole pair separation due to the formation of the Bi_2O_3/Bi_2SiO_5 nanoheterostructures. This work provides a principal method to produce bismuth-based mesoporous photocatalysts, and also a route to obtain an efficient photocatalyst for environmental purification.

Acknowledgements

This work was supported by the National Natural Science Foundation of China (51272303 and 50972155) and the 973 Program (2010CB933503).

References

1 M. D. Hernandez-Alonso, F. Fresno, S. Suarez and J. M. Coronado, *Environ. Sci. Technol.*, 2009, **2**, 1231–1257.
2 M. Anpo and M. Takeuchi, *J. Catal.*, 2003, **216**, 505–516.
3 A. T. Bell, *Science*, 2003, **299**, 1688–1691.
4 X. H. Zhang, W. Z. Li and H. Y. Xu, *Prog. Chem.*, 2004, **16**, 728–737.
5 Y. Horiuchi and H. Yamashita, *Appl. Catal., A*, 2011, **400**, 1–8.
6 M. S. Bazarjani, M. Hojamberdiev, K. Morita, G. Q. Zhu, G. Cherkashinin, C. Fasel, T. Herrmann, H. Breitzke, A. Gurlo and R. Riedel, *J. Am. Chem. Soc.*, 2013, **135**, 4467–4475.
7 J. Rosen, G. S. Hutchings and F. Jiao, *J. Am. Chem. Soc.*, 2013, **135**, 4516–4521.
8 Z. Zhou, A. W. Franz, M. Hartrnann, A. Seifert, T. J. J. Muller and W. R. Thiel, *Chem. Mater.*, 2008, **20**, 4986–4992.
9 S. Higashimoto, Y. Hu, R. Tsumura, K. Iino, M. Matsuoka, H. Yamashita, Y. G. Shul, M. Che and M. Anpo, *J. Catal.*, 2005, **235**, 272–278.
10 D. R. Sahu, L. Y. Hong, S. C. Wang and J. L. Huang, *Microporous Mesoporous Mater.*, 2009, **117**, 640–649.
11 A. N. Soon and B. H. Hameed, *Appl. Catal., A*, 2013, **450**, 96–105.
12 A. J. Ward, C. C. Weber, A. F. Masters and T. Maschmeyer, *ChemCatChem*, 2013, **5**, 959–965.
13 L. Zhao, Y. Chi, Q. Yuan, N. Li, W. F. Yan and X. T. Li, *J. Colloid Interface Sci.*, 2013, **390**, 70–77.
14 M. G. Kanatzidis, *Adv. Mater.*, 2007, **19**, 1165–1181.
15 J. N. Kondo and K. Domen, *Chem. Mater.*, 2008, **20**, 835–847.
16 Y. X. Liu, J. X. Shi, Q. Peng and Y. D. Li, *Chem.–Eur. J.*, 2013, **19**, 4319–4326.
17 C. L. Marchena, R. A. Frenzel, S. Gomez, L. B. Pierella and L. R. Pizzio, *Appl. Catal., B*, 2013, **130**, 187–196.
18 Z. Y. Wang, Z. C. Wang, H. B. Wu and X. W. Lou, *Sci. Rep.*, 2013, **3**, 1391.
19 C. Y. Zhang, S. B. Wang, H. J. Huo, Z. B. Huang, Y. Li, B. Z. Li and Y. G. Yang, *Chem.–Asian J.*, 2013, **8**, 709–712.
20 M. Kang, S. H. Yi, H. I. Lee, J. E. Yie and J. M. Kim, *Chem. Commun.*, 2002, 1944–1945.
21 W. Zhou, F. F. Sun, K. Pan, G. H. Tian, B. J. Jiang, Z. Y. Ren, C. G. Tian and H. G. Fu, *Adv. Funct. Mater.*, 2011, **21**, 1922–1930.
22 S. Y. Choi, M. Mamak, N. Coombs, N. Chopra and G. A. Ozin, *Adv. Funct. Mater.*, 2004, **14**, 335–344.
23 A. Hameed, T. Montini, V. Gombac and P. Fornasiero, *J. Am. Chem. Soc.*, 2008, **130**, 9658–9659.
24 S. Balachandran and M. Swaminathan, *J. Phys. Chem. C*, 2012, **116**, 26306–26312.
25 K. Brezesinski, R. Ostermann, P. Hartmann, J. Perlich and T. Brezesinski, *Chem. Mater.*, 2010, **22**, 3079–3085.
26 A. Walsh, G. Watson, D. Payne, R. Edgell, J. Guo, P.-A. Glans, T. Learmonth and K. Smith, *Phys. Rev. B: Condens. Matter Mater. Phys.*, 2006, **73**, 235104.
27 J. Q. Lu, X. F. Wang, C. L. Yu and Y. Q. Xu, *J. Mater. Sci.: Mater. Electron.*, 2012, **23**, 1770–1773.
28 L. Zhang, W. Z. Wang, S. M. Sun, J. H. Xu, M. Shang and J. Ren, *Appl. Catal., B*, 2010, **100**, 97–101.
29 H. W. Guo, X. F. Wang and D. N. Gao, *Mater. Lett.*, 2012, **67**, 280–282.
30 X. A. Feng, X. A. Qi, J. Li, L. W. Yang, M. C. Qiu, J. J. Yin, F. Lu and J. X. Zhong, *Appl. Surf. Sci.*, 2011, **257**, 5571–5575.
31 R. Chen, J. Bi, L. Wu, W. Wang, Z. Li and X. Fu, *Inorg. Chem.*, 2009, **48**, 9072–9076.
32 A. K. R. Police, S. Basavaraju, D. K. Valluri and S. Machiraju, *J. Mater. Sci. Technol.*, 2013, **29**, 639–646.
33 X. Huang, L. Shang, S. Chen, J. Xia, X. P. Qi, X. C. Wang, T. R. Zhang and X. M. Meng, *Nanoscale*, 2013, **5**, 3828–3833.
34 M. Gratzel, *Curr. Opin. Colloid Interface Sci.*, 1999, **4**, 314–321.
35 Y. Han and J. Y. Ying, *Angew. Chem., Int. Ed.*, 2005, **44**, 288–292.
36 J. Kaiser, *Science*, 2007, **317**, 884–885.
37 H. Melcer and G. Klecka, *Water Environ. Res.*, 2011, **83**, 650–666.
38 S. Wang, H. M. Ang and M. O. Tade, *Environ. Int.*, 2007, **33**, 694–705.
39 V. M. Denisov, L. A. Irtyugo and L. T. Denisova, *Phys. Solid State*, 2011, **53**, 2180–2182.
40 G. Z. Shen and D. Chen, *Recent Pat. Nanotechnol.*, 2010, **4**, 20–31.
41 T. Zhai, L. Li, X. Wang, X. S. Fang, Y. Bando and D. Golberg, *Adv. Funct. Mater.*, 2010, **20**, 4233–4248.

